Geophysical Research Letters

RESEARCH LETTER
10.1029/2019GL081898

Precipitation From Persistent Extremes is Increasing in Most Regions and Globally

Haibo Du[1,2], Lisa V. Alexander[3], Markus G. Donat[3,4], Tanya Lippmann[3,5], Arvind Srivastava[6], Jim Salinger[7], Andries Kruger[8,9], Gwangyong Choi[10], Hong S. He[1,2], Fumiaki Fujibe[11], Matilde Rusticucci[12], Banzragch Nandintsetseg[13,14], Rodrigo Manzanas[15], Shafiqur Rehman[16], Farhat Abbas[17], Panmao Zhai[18], Ibouraïma Yabi[19], Michael C. Stambaugh[2], Shengzhong Wang[1], Altangerel Batbold[14], Priscilla Teles de Oliveira[20], Muhammad Adrees[17], Wei Hou[21], Shengwei Zong[1], Claudio Moises Santos e Silva[22], Paulo Sergio Lucio[22], and Zhengfang Wu[1]

[1]Key Laboratory of Geographical Processes and Ecological Security in Changbai Mountains, Ministry of Education, School of Geographical Sciences, Northeast Normal University, Changchun, China, [2]School of Natural Resource, University of Missouri, Columbia, MO, USA, [3]Climate Change Research Centre and ARC Centre of Excellence for Climate Extremes, University of New South Wales, Sydney, New South Wales, Australia, [4]Barcelona Supercomputing Center, Barcelona, Spain, [5]Department of Earth Sciences, Faculty of Earth and Life Sciences, Vrije Universiteit Amsterdam, Amsterdam, Netherlands, [6]National Climate Centre, India Meteorological Department, Pune, India, [7]Tasmanian Institute of Agriculture, University of Tasmania, Hobart, Tasmania, Australia, [8]Climate Service, South African Weather Service, Pretoria, South Africa, [9]Department of Geography, Geoinformatics and Meteorology, Faculty of Natural and Agricultural Sciences, University of Pretoria, Pretoria, South Africa, [10]Major of Geography Education, Jeju National University, Jeju-si, South Korea, [11]Department of Geography, Tokyo Metropolitan University, Hachioji, Japan, [12]Departamento de Ciencias de la Atmósfera y los Océanos, Universidad de Buenos Aires/CONICET, Buenos Aires, Argentina, [13]School of Arts and Sciences, National University of Mongolia, Ulaanbaatar, Mongolia, [14]Information and Research Institute of Meteorology, Hydrology and Environment, Ulaanbaatar, Mongolia, [15]Meteorology Group, Institute of Physics of Cantabria (IFCA), CSIC-University of Cantabria, Santander, Spain, [16]Center for Engineering Research, Research Institute, King Fahd University of Petroleum and Minerals, Dhahran, Saudi Arabia, [17]Department of Environmental Sciences and Engineering, Government College University, Faisalabad, Pakistan, [18]State Key Laboratory of Severe Weather, Chinese Academy of Meteorological Sciences, Beijing, China, [19]Laboratory of Climatology, Department of Geography and Planning, University of Abomey-Calavi, Abomey-Calavi, Benin, [20]Faculdade de Ciências, Universidade Estadual Paulista, São Paulo, Brazil, [21]National Climate Center, China Meteorological Administration, Beijing, China, [22]Programa de Pós-Graduação em Ciências Climáticas, Universidade Federal do Rio Grande do Norte, Natal, Brazil

Key Points:
- Precipitation from persistent extremes is increasing in most global land regions
- Globally observed and modeled persistent precipitation maxima relative increases are lower compared to daily extremes
- The increases in annual-maximum persistent precipitation per degree global warming across models are independent of the emissions scenario

Supporting Information:
- Supporting Information S1

Correspondence to:
Z. Wu,
wuzf@nenu.edu.cn

Citation:
Du, H., Alexander, L. V., Donat, M. G., Lippmann, T., Srivastava, A., Salinger, J., et al. (2019). Precipitation from persistent extremes is increasing in most regions and globally. *Geophysical Research Letters*, *46*, 6041–6049. https://doi.org/10.1029/2019GL081898

Received 11 NOV 2018
Accepted 17 MAY 2019
Accepted article online 21 MAY 2019
Published online 7 JUN 2019

Abstract Extreme precipitation often persists for multiple days with variable duration but has usually been examined at fixed duration. Here we show that considering extreme persistent precipitation by complete event with variable duration, rather than a fixed temporal period, is a necessary metric to account for the complexity of changing precipitation. Observed global mean annual-maximum precipitation is significantly stronger (49.5%) for persistent extremes than daily extremes. However, both globally observed and modeled rates of relative increases are lower for persistent extremes compared to daily extremes, especially for Southern Hemisphere and large regions in the 0-45°N latitude band. Climate models also show significant differences in the magnitude and partly even the sign of local mean changes between daily and persistent extremes in global warming projections. Changes in extreme precipitation therefore are more complex than previously reported, and extreme precipitation events with varying duration should be taken into account for future climate change assessments.

1. Introduction

The global hydrological cycle is expected to intensify with warming (Allen & Ingram, 2002), which will likely increase the intensity of daily extreme precipitation (Intergovernmental Panel on Climate Change, 2013). Observed globally averaged precipitation extremes show widespread statistically significant increasing trends (Alexander et al., 2006; Donat, Alexander, Yang, Durre, Vose, Dunn, et al., 2013), which are expected to continue into the future (Sillmann et al., 2013). Both observations and models agree that extreme daily precipitation increases also at regional scales when averaged over either the wetter or the drier parts of land areas (Donat et al., 2016). However, understanding the changes in precipitation extremes is complex and can

depend on their predetermined definitions. Many ways are used to define extreme precipitation, and the choice of definition of a particular index affects how it responds to climate warming (Pendergrass, 2018). Most studies analyzed extreme precipitation using rainfall amounts over temporal window (e.g., one-day (Du et al., 2013; O'Gorman, 2012)) or over multiday periods of fixed duration (Chen & Zhai, 2013), rather than considering the rainfall amount of a complete precipitation event with varying durations. While some precipitation events occur within one day, others persist for time periods longer than one day (Chen & Zhai, 2016; Liu & Wu, 2016). Analyses by fixed-period precipitation indices do not consider the actual situation that precipitation includes events of different durations. This indicates that changes in extreme precipitation may be more complex than accounted for in analyses of fixed-duration extremes. The influence of climate change on global extreme persistent precipitation (the maximum precipitation of a complete precipitation event with varying duration) has not been fully assessed yet in observations or climate model simulations.

The change in extreme precipitation is often expected to scale with precipitable water changes under warming climate if relative humidity and precipitation efficiency remain constant and atmospheric circulation does not change considerably (Lenderink & van Meijgaard, 2008, 2010). Using the Clausius-Clapeyron relation to predict precipitation extremes is considered a better approach than using mean precipitation changes (Allen & Ingram, 2002; Emori & Brown, 2005). However, precipitation extremes scaling with temperature change can be different among various timescales of precipitation accumulation (Guerreiro et al., 2018), as well as among different regions (Kharin et al., 2013) mainly due to different changes in dynamics (Pfahl et al., 2017). Most of these studies focused on fixed-duration (e.g., hourly or 1 day) precipitation. The changes in extreme persistent precipitation may differ from those in the fixed daily events. How extreme persistent precipitation changes in a warming climate relative to extreme daily precipitation and mean precipitation is up to now unknown.

The main obstacle to answering the above research questions was initially a lack of availability of high-quality, long-term observed daily precipitation data covering large portions of the world (Alexander et al., 2006). Although internationally coordinated efforts have worked to address some gaps in data availability (Donat, Alexander, Yang, Durre, Vose, & Caesar, 2013; Donat, Alexander, Yang, Durre, Vose, Dunn, et al., 2013; Durre et al., 2018), the data coverage remained poor in many regions, especially in Africa and South America. For this reason, this study has striven to bring together as many data contributors and coauthors, now representing fifteen countries. These contributions provide a unique and long-term (1961-2010) observational data set covering most of the global land area, except for large parts of Africa (see section 2 for details). This comprehensive data set is expected to allow an improved understanding of changing extreme daily and persistent precipitation events. Here we analyze the annual-maximum precipitation amounts associated with daily and persistent precipitation events (see section 2 for details).

2. Data and Methods

2.1. Observations

To provide the most comprehensive analysis of observed global extreme persistent precipitation, we use high-quality daily precipitation data from a number of different sources. Coauthors from 15 countries contributed daily data, most of which until now were not available for global precipitation studies. The compilation of global daily precipitation data includes the GHCND data set (Menne et al., 2012); the ECA&D data set (Klein Tank et al., 2002); raw data provided by authors from Argentina, Australia, Benin, Brazil, India, Japan, Korea, Mongolia, Pakistan, South Africa, Saudi Arabia, Spain, Russia, and the United States (Menne et al., 2010), and homogenized data from Canada (Vincent et al., 2012), China (author), and New Zealand (author). In total, 12,151 stations were collated (Figure S1a in the supporting information). After quality control and homogeneity tests, 6,125 high-quality stations with long-term daily precipitation for the period 1961-2010 remained for the study (Text S1 and Figure S1b in the supporting information).

2.2. Coupled Model Intercomparison Project Phase 5 Model Simulations

This analysis uses historical simulations and future projections from 30 Coupled Model Intercomparison Project Phase 5 (CMIP5) models. Two future Representative Concentration Pathways (RCP4.5 and RCP8.5) are used as moderate and high forcing scenarios to simulate possible future changes in extreme precipitation (Table S1 in the supporting information).

2.3. Definition of Persistent Precipitation

Many precipitation events persist for longer than 1 day. For example, a precipitation event begins on one day and ends the next. Extreme precipitation may not be recorded in just 1 day, but the 2-day persistent precipitation can be considered an extreme event, because the total amount of both days may pose substantial risk (Merino et al., 2018). However, sometimes such a persistent event contains days with light precipitation amounts, and we note that it may not rain unintermittently throughout a day even when accumulations over a day or multiple days are substantial. The days with lighter precipitation amounts can increase the duration of the persistent precipitation event but may not substantially increase the total precipitation amount. Therefore, we only consider persistent precipitation events during which all days exceed a moderate precipitation amount on average. We use the average daily precipitation amount (calculated using wet days during 1961-1990) as a criterion to construct persistent precipitation series from daily precipitation series. As an example, assume that the precipitation amounts of 10 days of a (simulated or observed) daily precipitation series are represented by a, a, 0, b, a, 0, b, b, a, and b, respectively, where a indicates that the precipitation on that day is less than the required average precipitation amount. Conversely, b indicates daily precipitation above average. The value of zero indicates nonprecipitation on that day. The precipitation of consecutive b days is treated as one persistent precipitation event for this maximum persistent precipitation analysis. This means the 10-day daily precipitation series may be written as a new persistent precipitation series: a, a, 0, b, a, 0, consecutive b (persistent for two days), a, and b. This persistent precipitation series is then used to calculate maximum persistent precipitation events in a following step.

2.4. Annual Maximum Precipitation From Observations and the CMIP5 Models

We construct the persistent precipitation time series using the method described above, and then calculate the annual-maximum precipitation of persistent precipitation events (RxEvent) and the annual-maximum precipitation of daily series (Rx1day) for both observational station data and the CMIP5 simulations. The observed annual Rx1day and RxEvent are bilinearly interpolated onto a 2° × 2° grid. This order of operation (gridding station annual precipitation index time series) is similar to the process of existing studies of quasi-global data sets of temperature and precipitation extremes (e.g., HadEX2 (Donat, Alexander, Yang, Durre, Vose, Dunn, et al., 2013) and GHCNDEX (Donat, Alexander, Yang, Durre, Vose, & Caesar, 2013)), calculating the extreme precipitation indices before interpolating the indices. Grid boxes without an observational station within a 2° circumference are defined as a missing value for observed data. Uninhabited regions (high southern latitudes [south of 60° S]) and ocean that are not subjected to pluvial flooding are excluded from the analyses.

We note that different orders of operation by calculating precipitation maxima from gridded or station daily time series may have different results due to possible scale dependence (Avila et al., 2015). Therefore, we also investigate the changes in the observed Rx1day and RxEvent calculated using daily grids (Text S2 and Figures S6 and S7) to check possible scale dependence and test the sensitivity of the results to the order of operations, and we find that results are generally very similar and our conclusions robust regardless of which order of operations is used. We therefore decide to base the main text results on the approach with first calculating annual maxima in the station data before gridding, because of concerns about the representativeness of daily precipitation grids at 2° × 2° resolutions on the one hand, but distribution and density of stations possibly not allowing robust daily precipitation grids at higher spatial resolution.

2.5. Analysis of Long-Term Changes

Annual indices are normalized by dividing by the climatological mean (1961-2010 for observations; 1961-2005 for models) for each grid box, and the global average before trends are calculated. The ordinary least squares method is used to calculate the temporal trends of annual-maximum precipitation for each grid box, and for the global average time series. The significance of the trend is estimated by the nonparametric Mann-Kendall test. The significance of the local (grid cell) difference between Rx1day and RxEvent is tested by the Wilcoxon signed rank test. The simulated local and regional changes are considered as "robust change" when more than 50% of the models show significant ($p \leq 0.05$) change and at least 80% of those agree on the sign of change (Tebaldi et al., 2011).

2.6. Temperature-Precipitation Scaling Relationship

We calculate the respective differences of temperature and precipitation index averages between two periods (2071-2100 relative to 1961-2005) for individual models. We then investigate whether precipitation changes are related to global temperature changes across models using the ordinary least squares regression. The significance of the regression relationship is estimated by the Mann-Kendall test.

2.7. Uncertainties of Changes in Maximum Precipitation Across the CMIP5 Models

We first calculate local trends of the projections for individual models. We then calculate the standard deviation (*SD*) of the changes across all models used in this study. A large *SD* indicates that the differences among the multimodel projections are large, which also denotes large uncertainty, and vice versa.

3. Results

3.1. Observed and Simulated Historical Mean Spatial Distribution and Changes

Global spatial patterns averaged over the 1961-2010 period are similar between annual-maximum precipitation of daily series (Rx1day) and annual-maximum total precipitation of persistent precipitation events (RxEvent) but differ in magnitude at regional scales (Figure 1). Both intense mean Rx1day and RxEvent (e.g., ≥100 mm) are observed in Southeast Asia, Southeast America, North-eastern Australia, and parts of South America, while low extreme events are shown in central Asia and the Northern Hemisphere high latitudes, where both Rx1day and RxEvent are less than 30 mm (Figure 1). However, the globally averaged RxEvent is significantly ($p \leq 0.01$; see section 2) stronger with 49.5% (77.0 mm versus 51.5 mm) than Rx1day, which is expected as the fixed-duration metric may divide a real multiday precipitation event into several separate one-day precipitation events. Historical simulations of CMIP5 models slightly underestimate global mean Rx1day (30.7 [22.5-41.3] mm) but produce a similar global mean RxEvent (72.9 [62.0-89.0] mm) for the observational spatial coverage (Figure S2). The observed high long-term average of maximum precipitation (≥100 mm) occurs within 23.6% of grid boxes for RxEvent, which are obviously more than for Rx1day (only 9.7% of grid boxes). These results indicate that separately considering 1-day maximum precipitation extremes may affect risk assessments related to extreme precipitation events that actually persist for days.

Globally averaged observations show that the significant increasing trend of RxEvent (0.65% per decade) is smaller than the significant increasing trend in Rx1day (0.85% per decade; Figure 2d). This means that on average, although mean RxEvent is significantly stronger than mean Rx1day, the maximum precipitation of a persistent precipitation event is becoming intense but slower in relation to maximum daily precipitation. The difference is confirmed by the results from the CMIP5 historical simulations (Figure S3).

Although the area-average time series of both observed Rx1day and RxEvent show increases, they contain local decreasing changes in some areas, for example, in Western North America, parts of Eastern Asia, and Eastern Australia (Figures 2a and 2b). However, most of the local change signs are the same between persistent and daily maxima, for example, with increasing trend in most of Europe, but changes of opposing sign are found at a few grid cells in parts of South America. The spatial patterns of the differences of the trends between RxEvent and Rx1day are subsequently investigated (Figure 2c). Decreasing trends in the difference series of RxEvent minus Rx1day are found in many areas, for example, in Western America, India, North China, most Japan, most of Brazil, and most of Australia (generally in large areas in region of 45°S-45°N; Figure 2c).

3.2. Projected Precipitation Maxima Spatial Distribution and Changes

Relatively high mean Rx1day and RxEvent during 2006-2100 are predominant in tropical regions for projected scenarios (Figure S4). The global long-term mean annual maximum precipitation is 31.6 (RCP4.5) and 33.1 (RCP8.5) mm for Rx1day and 85.6 (RCP4.5) and 87.5 (RCP8.5) mm for RxEvent (Figure S4). That is, the average annual-maximum precipitation of the projected persistent precipitation event is stronger by a factor ~2.7 (2.64 (RCP8.5) and 2.71 (RCP4.5)) than that of daily precipitation during 2006-2100. The temporal changes of ensemble-mean indices are calculated over the period 2006-2100 (Figure 3). Higher radiative forcing scenarios cause stronger increasing trends in both Rx1day and RxEvent compared to lower radiative forcing scenarios. In agreement with the observed changes, the projected global land average trends of RxEvent are slightly lower than the trends of Rx1day for both scenarios (Figures 3a and 3b).

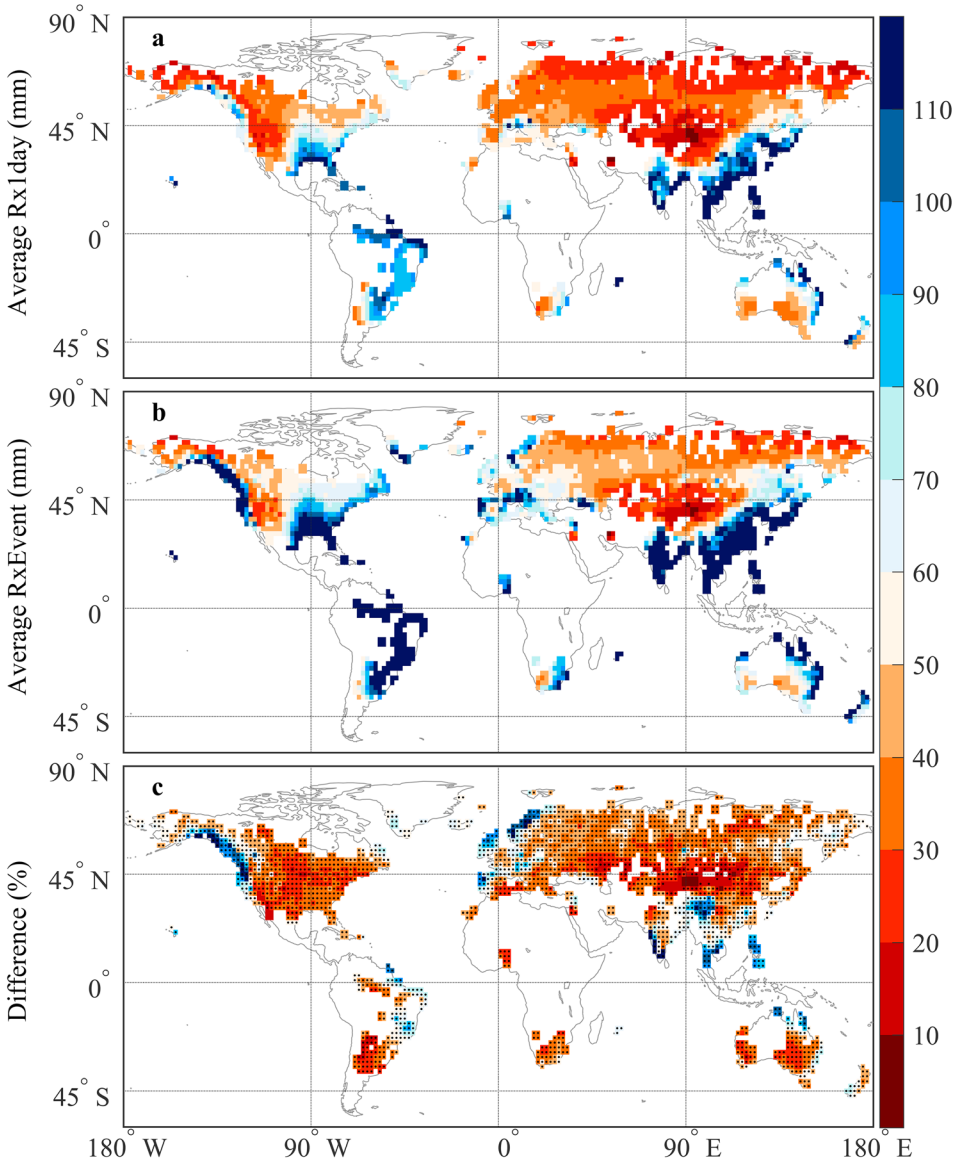

Figure 1. Global spatial distribution of observed long-term mean annual maximum precipitation during 1961-2010. (a) Rx1day (the annual-maximum daily precipitation); (b) RxEvent (the annual-maximum total precipitation of persistent precipitation event); (c) the difference as a percentage of RxEvent minus Rx1day divided by Rx1day. Stippling in (c) means the local difference is significant ($p \leq 0.05$) by the Wilcoxon signed rank test. The blank grid boxes represent areas with no data.

Under future climate projections, both Rx1day and RxEvent are projected to be increasing for most land for both scenarios, except for parts of Southern and Northern Africa (Figures 3d, 3e, 3g, and 3h). Strongly increasing trends in Rx1day and RxEvent are most predominant within Southeast Asia, Northeast Asia, most of India, Eastern Africa, Eastern Brazil, Alaska, and Greenland. However, the spatial patterns are heterogeneous to the extent that certain regions may exhibit changes of opposing signs between the spatial patterns of Rx1day and RxEvent. Opposing trends are shown at a few locations in Central Africa and parts of Northern Latin America, with increasing trend for Rx1day but decreasing trend for RxEvent. That is, the annual-maximum precipitation of persistent precipitation event is simulated to weaken, while the annual-maximum precipitation of daily precipitation is simulated to intensify in these regions. The increasing trends are weaker for RxEvent than Rx1day in most areas in Southern Hemisphere and parts in 0°-45°N but stronger for RxEvent than Rx1day north of 45°N (Figures 3f and 3i). Despite the partly inconsistent spatial

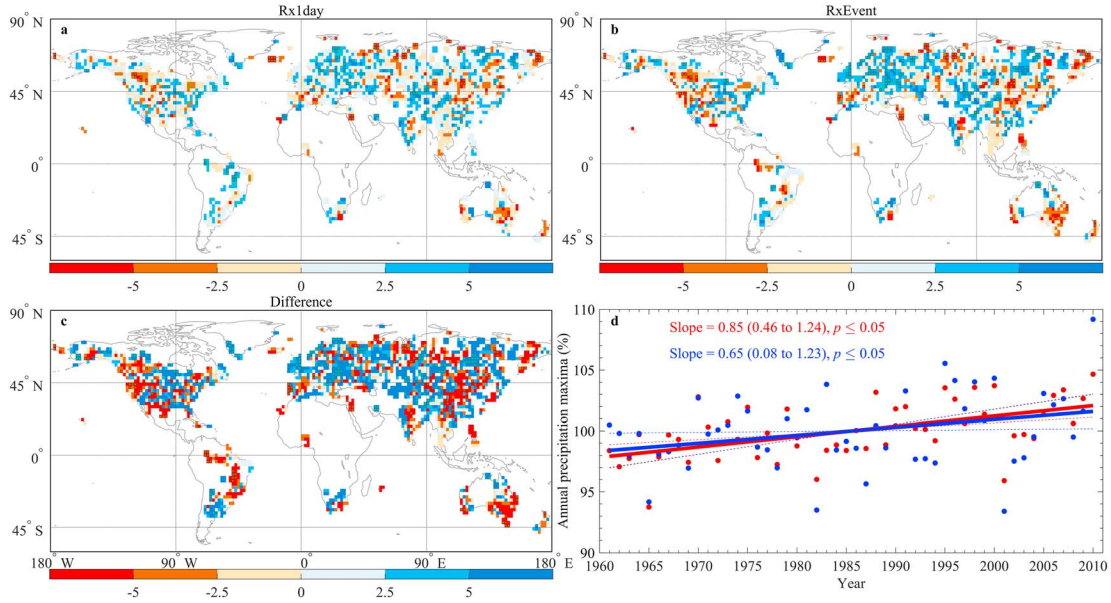

Figure 2. Local and regional trends (% per decade) in the annual maximum precipitation from observations during 1961-2010. Local trends in (a) Rx1day (the annual-maximum daily precipitation), (b) RxEvent (the annual-maximum total precipitation of persistent precipitation event), and (c) the trends of the difference time series (RxEvent minus Rx1day). (d) Global time series in Rx1day (red) and RxEvent (blue). Both indices are normalized by calculating annual values as a percentage of the mean in 1961-2010 before calculating trends. The green stippling in (a)–(c) means a significant trend ($p \leq 0.05$) by the Mann-Kendall test. The blank grid boxes represent no data.

patterns of local changes, averaging over larger areas removes much of the local-scale noise (Donat et al., 2016; Fischer et al., 2013) and leads to a robust global mean change (Figures 3a–3c).

The Rx1day/RxEvent-temperature scaling relationships across models are calculated over the period 2006-2100 (Figure 4). The increases in global land mean Rx1day and RxEvent against global land surface

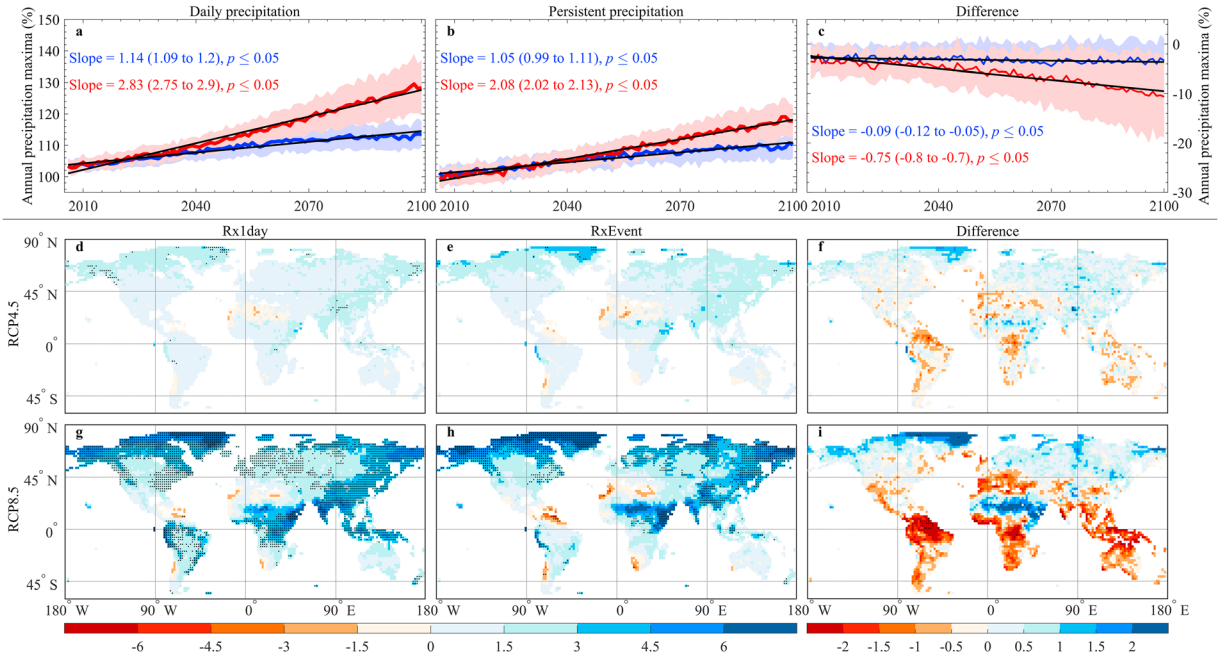

Figure 3. Same as Figure 2 but for the trends in Rx1day/RxEvent during 2006-2100 for the RCP4.5 and RCP8.5 scenarios. The reference value for normalization is the mean index value from the historical simulations during 1961-2005. (a–c) The time series for RCP4.5 (blue) and RCP8.5 (red) scenarios; the colored shadings indicate ± one ensemble standard deviation. Stippling in (d)–(i) indicates "robust change" across all models (see section 2).

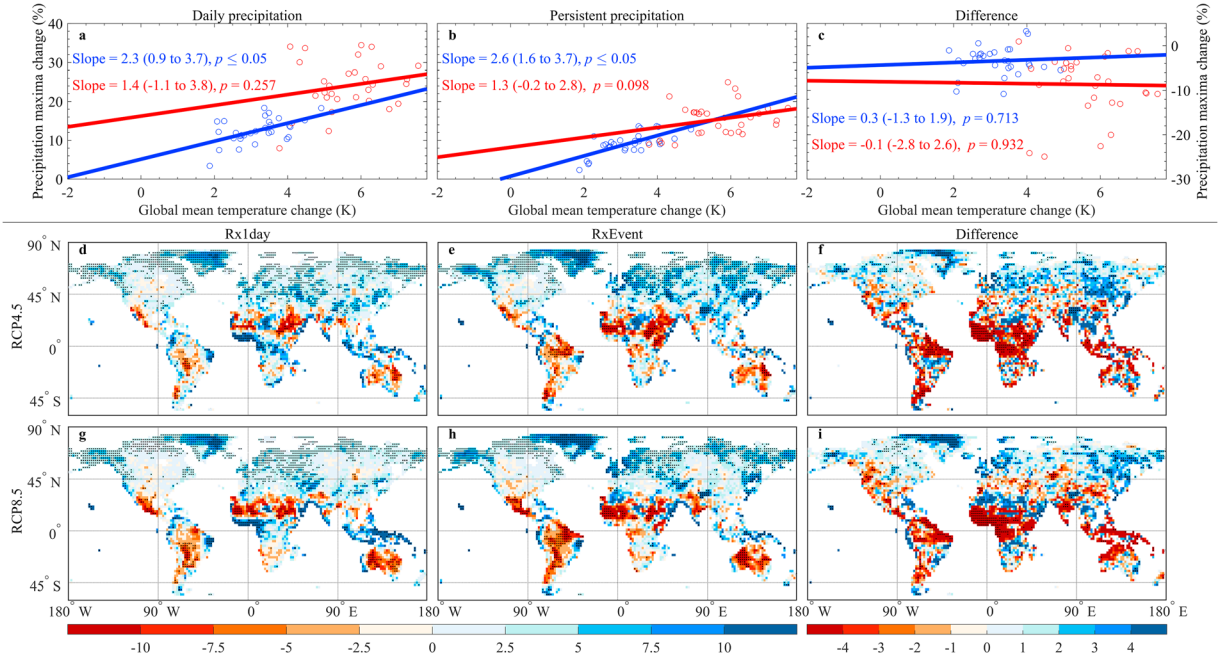

Figure 4. Linear regression relationships (% per K) between projected mean temperature change and mean annual-maximum precipitation change across all models. Rx1day is the annual-maximum daily precipitation; RxEvent is the annual-maximum total precipitation of persistent precipitation. The temperature and precipitation changes are the average in 2071-2100 relative to the respective mean during 1961-2005. (a–c) Scatter plots of global mean precipitation maxima change against global land mean temperature change for Rx1day (up left), RxEvent (up middle), and the difference, that is, RxEvent minus Rx1day (up right) for RCP4.5 (blue) and RCP8.5 (red) scenarios respectively. Each point represents the changes between two periods for individual models. (d–i) Spatial patterns of the regression relationships between grid cell mean temperature change and mean annual-maximum precipitation change for (d and g) Rx1day, (e and h) RxEvent, and (f and i) the difference. Stippling represents a significant regression relationship ($p \leq 0.05$) by the Mann-Kendall test.

temperature increase are both lower than the Clausius-Clapeyron relationship (by increasing 6-7% per K of warming; Allen & Ingram, 2002). The global average Rx1day/RxEvent-temperature scaling relationships overlap each other's confidence intervals (95%) between both scenarios (Figures 4a–4c), indicating that the changes in annual-maximum precipitation per degree warming appear independent of scenario. The increase of precipitation maxima depends primarily on the magnitude of warming (Figure 3) and not on the composition of the change in forcing in future (Pendergrass et al., 2016). This confirms the stability of pattern scaling of the externally forced changes in precipitation under warming across scenarios (Tebaldi & Arblaster, 2014).

For changes at grid cell level, models with stronger simulated warming show weaker increases in Rx1day and RxEvent within south-western North America, most of South America, most regions in Northern Africa, parts in Southern Africa, large regions of India (for RxEvent for RCP8.5 scenario), and most of Australia, but stronger increases in most other regions (Figures 4d–4i). Similar to the trends in Rx1day/RxEvent (Figure 3), opposing temperature-precipitation relationships between Rx1day and RxEvent are also shown at a few locations in Central Africa, parts of Northern Latin America, and Northern India, with positive regression coefficients for Rx1day but negative for RxEvent. More generally, the increases in Rx1day and RxEvent are weaker for models with stronger simulated warming in the Southern Hemisphere and large regions in the 0°-45°N zone, but stronger in other regions over the 21st century for both RCP4.5 and RCP8.5 scenarios. Comparably, the negative RxEvent-temperature relationships are stronger than the negative Rx1day-temperature relationships in large regions south of 45°N, resulting in significant decreases in the difference of RxEvent minus Rx1day against simulated stronger warming (across models) for large areas in this region (Figures 4f and 4i). This is very similar to the patterns of trend differences in the annual-maximum precipitation between daily precipitation and persistent precipitation events (Figures 3f and 3i).

The spatial patterns of the intermodel uncertainty are similar between Rx1day and RxEvent, whereas the model uncertainty of simulated trends is larger for the higher radiative forcing scenario than for the lower

radiative forcing scenario (Figure S5). The globally averaged model uncertainty is larger for RxEvent than for Rx1day in both scenarios. The smallest uncertainties are primarily to the north of 45°N for both indices and both scenarios. The largest uncertainties are mainly in the tropics and subtropics, especially for Northern Africa, in part due to relevant climatic processes for precipitation being subject to subgrid parameterizations (Wilcox & Donner, 2007), and sparse observations in these areas (O'Gorman, 2012). Also, changes in precipitation may be attributed to contributions from changes in atmospheric thermodynamics and dynamics (Allen & Ingram, 2002; O'Gorman, 2015). The dynamic contribution is large over the tropics and subtropics, which amplifies or weakens the spatially homogeneous changes in extreme precipitation by thermodynamics (Pfahl et al., 2017), also adding to the differences within the model ensemble in these regions.

4. Conclusions

In this study, we combine a new global data set based on in situ observations as well as modeled data to explore changes in the annual-maximum precipitation of persistent precipitation events (RxEvent) relative to daily precipitation (Rx1day) over global land areas over the past 50 years (1961-2010) and projections of 21st century. Long-term average RxEvent is statistically significantly stronger than Rx1day for both observations (by a factor of 1.5) and future projections (by a factor of 2.7). However, both observations and projections show lower rates of relative increases for globally averaged RxEvent than for Rx1day. This is primarily because the relative increases in RxEvent are slower than increases in Rx1day in Southern Hemisphere and large regions in 0°-45°N during the last 50 years and the differences will continue to during 21st century, although RxEvent increases faster in most areas of north of 45°N. Moreover, opposite changes between Rx1day and RxEvent are shown in parts of Northern Latin America, Central Africa, and Northern India. The increases in Rx1day/RxEvent per degree global warming across models are independent of the emissions scenario, and the maximum precipitation differences in time series by end of 21st century are mainly due to stronger forcing. However, regional spatial patterns projected by models are heterogeneous for the changes in maximum precipitation to the extent that different regions may exhibit changes of opposing signs. Regionally, the increase in RxEvent is weaker than the increase in Rx1day for models with simulated stronger warming in large areas to the south of 45°N. Uncertainties associated with expected changes of the annual-maximum precipitation of multimodel simulations are larger in the tropics and subtropics than for other regions. This shows that further work is required to fill knowledge gaps and decrease uncertainties.

Analyses of this in situ data collection provide insight into how global annual precipitation maxima are changing in a warming world. Further studies are needed to better understand the regional spatial heterogeneity of changes in extreme persistent precipitation to be expected with a warming climate. A particular focus on regional changes and the identification of regional contributions to global-scale changes is necessary to improve our understanding of the complex changes in extreme precipitation. This study advocates that persistent precipitation totals should be a necessary component of this work.

Acknowledgments

Data Set names: the CMIP5 data set (http://pcmdi9.llnl.gov/), the GHCND data set (https://www.ncdc.noaa.gov/ghcn-daily-description), the ECA&D data set (https://www.ecad.eu/), the USHCN data set (http://cdiac.ess-dive.lbl.gov/ftp/ushcn_daily/), and the data set for Canada (http://climate.weather.gc.ca/). Observed data set is available online (https://doi.org/10.5281/zenodo.2573295). This work is jointly supported by the National Key R&D Program of China (2016YFA0602301), National Natural Science Foundation of China (41601052), Science and Technology Development Plan of Jilin Province (20190201291JC and 20180520098JH), the Spanish Ministry for the Economy, Industry and Competitiveness Ramón y Cajal 2017 (RYC-2017-22964), the EU Horizon 2020 EUCP project (776613), and National University of Mongolia (P2017-2504).

References

Alexander, L. V., Zhang, X., Peterson, T. C., Caesar, J., Gleason, B., Klein Tank, A. M. G., et al. (2006). Global observed changes in daily climate extremes of temperature and precipitation. *Journal of Geophysical Research*, *111*, D05109. https://doi.org/10.1029/2005JD006290

Allen, M. R., & Ingram, W. J. (2002). Constraints on future changes in climate and the hydrologic cycle. *Nature*, *419*(6903), 224–232. https://doi.org/10.1038/nature01092

Avila, F. B., Dong, S., Menang, K. P., Rajczak, J., Renom, M., Donat, M. G., & Alexander, L. V. (2015). Systematic investigation of gridding-related scaling effects on annual statistics of daily temperature and precipitation maxima: A case study for south-east Australia. *Weather and Climate Extremes*, *9*, 6–16. https://doi.org/10.1016/j.wace.2015.06.003

Chen, Y., & Zhai, P. (2013). Persistent extreme precipitation events in China during 1951-2010. *Climate Research*, *57*(2), 143–155.

Chen, Y., & Zhai, P. (2016). Mechanisms for concurrent low-latitude circulation anomalies responsible for persistent extreme precipitation in the Yangtze River Valley. *Climate Dynamics*, *47*(3), 989–1006. https://doi.org/10.1007/s00382-015-2885-6

Donat, M. G., Alexander, L. V., Yang, H., Durre, I., Vose, R., & Caesar, J. (2013). Global land-based datasets for monitoring climatic extremes. *Bulletin of the American Meteorological Society*, *94*(7), 997–1006. https://doi.org/10.1175/bams-d-12-00109.1

Donat, M. G., Alexander, L. V., Yang, H., Durre, I., Vose, R., Dunn, R. J. H., et al. (2013). Updated analyses of temperature and precipitation extreme indices since the beginning of the twentieth century: The HadEX2 dataset. *Journal of Geophysical Research: Atmospheres*, *118*, 2098–2118. https://doi.org/10.1002/jgrd.50150

Donat, M. G., Lowry, A. L., Alexander, L. V., O'gorman, P. A., & Maher, N. (2016). More extreme precipitation in the world's dry and wet regions. *Nature Climate Change*, *6*(5), 508–513. https://doi.org/10.1038/nclimate2941

Du, H., Wu, Z., Zong, S., Meng, X., & Wang, L. (2013). Assessing the characteristics of extreme precipitation over northeast China using the multifractal detrended fluctuation analysis. *Journal of Geophysical Research: Atmospheres*, *118*, 6165–6174. https://doi.org/10.1002/jgrd.50487

Durre, I., Yin, X., Vose, R. S., Applequist, S., & Arnfield, J. (2018). Enhancing the data coverage in the integrated global radiosonde archive. *Journal of Atmospheric and Oceanic Technology*, *35*, 1753–1770. https://doi.org/10.1175/JTECH-D-17-0223.1

Emori, S., & Brown, S. J. (2005). Dynamic and thermodynamic changes in mean and extreme precipitation under changed climate. *Geophysical Research Letters*, *32*, L17706. https://doi.org/10.1029/2005GL023272

Fischer, E., Beyerle, U., & Knutti, R. (2013). Robust spatially aggregated projections of climate extremes. *Nature Climate Change*, *3*(12), 1033–1038. https://doi.org/10.1038/nclimate2051

Guerreiro, S. B., Fowler, H. J., Barbero, R., Westra, S., Lenderink, G., Blenkinsop, S., et al. (2018). Detection of continental-scale intensification of hourly rainfall extremes. *Nature Climate Change*, *8*(9), 803–807. https://doi.org/10.1038/s41558-018-0245-3

Intergovernmental Panel on Climate Change (2013). *Climate change 2013: The physical science basis, Contribution of Working Group I to the Fifth Assessment Report of the Intergovernmental Panel on Climate Change*, edited by T. F. Stocker et al., Cambridge University Press, Cambridge, U. K., and New York.

Kharin, V. V., Zwiers, F. W., Zhang, X., & Wehner, M. (2013). Changes in temperature and precipitation extremes in the CMIP5 ensemble. *Climatic Change*, *119*(2), 345–357. https://doi.org/10.1007/s10584-013-0705-8

Klein Tank, A. M. G., Wijngaard, J. B., Können, G. P., Böhm, R., Demarée, G., Gocheva, A., et al. (2002). Daily dataset of 20th-century surface air temperature and precipitation series for the European Climate Assessment. *International Journal of Climatology*, *22*(12), 1441–1453. https://doi.org/10.1002/joc.773

Lenderink, G., & van Meijgaard, E. (2008). Increase in hourly precipitation extremes beyond expectations from temperature changes. *Nature Geoscience*, *1*(8), 511–514. https://doi.org/10.1038/ngeo262

Lenderink, G., & van Meijgaard, E. (2010). Linking increases in hourly precipitation extremes to atmospheric temperature and moisture changes. *Environmental Research Letters*, *5*(2), 025208. https://doi.org/10.1088/1748-9326/5/2/025208

Liu, G., & Wu, R. (2016). Spatial and temporal characteristics of summer precipitation events spanning different numbers of days over Asia. *International Journal of Climatology*, *36*(5), 2288–2302. https://doi.org/10.1002/joc.4495

Menne, M. J., Durre, I., Vose, R. S., Gleason, B. E., & Houston, T. G. (2012). An overview of the Global Historical Climatology Network-Daily Database. *Journal of Atmospheric and Oceanic Technology*, *29*(7), 897–910. https://doi.org/doi:10.1175/JTECH-D-11-00103.1

Menne, M. J., Williams, C. N. Jr., & Vose, R. S. (2010). *Long-term daily and monthly climate records from stations across the Contiguous United States*. Retrieved from http://cdiac.ornl.gov/epubs/ndp/ushcn/access.html, (accessed 23 September 2010).

Merino, A., Fernández-González, S., García-Ortega, E., Sánchez, J. L., López, L., & Gascón, E. (2018). Temporal continuity of extreme precipitation events using sub-daily precipitation: application to floods in the Ebro basin, northeastern Spain. *International Journal of Climatology*, *38*(4), 1877–1892. https://doi.org/doi:10.1002/joc.5302

O'Gorman, P. A. (2012). Sensitivity of tropical precipitation extremes to climate change. *Nature Geoscience*, *5*(10), 697–700. https://doi.org/10.1038/ngeo1568

O'Gorman, P. A. (2015). Precipitation extremes under climate change. *Current Climate Change Reports*, *1*(2), 49–59. https://doi.org/10.1007/s40641-015-0009-3

Pendergrass, A. G. (2018). What precipitation is extreme? *Science*, *360*(6393), 1072–1073. https://doi.org/10.1126/science.aat1871

Pendergrass, A. G., Lehner, F., Sanderson, B. M., & Xu, Y. (2016). Does extreme precipitation intensity depend on the emissions scenario? *Geophysical Research Letters*, *42*, 8767–8774. https://doi.org/10.1002/2015GL065854

Pfahl, S., O'Gorman, P. A., & Fischer, E. M. (2017). Understanding the regional pattern of projected future changes in extreme precipitation. *Nature Climate Change*, *7*(6), 423–427. https://doi.org/10.1038/nclimate3287

Sillmann, J., Kharin, V. V., Zwiers, F. W., Zhang, X., & Bronaugh, D. (2013). Climate extremes indices in the CMIP5 multimodel ensemble: Part 2. Future climate projections. *Journal of Geophysical Research: Atmospheres*, *118*, 2473–2493. https://doi.org/10.1002/jgrd.50188

Tebaldi, C., & Arblaster, J. M. (2014). Pattern scaling: Its strengths and limitations, and an update on the latest model simulations. *Climatic Change*, *122*(3), 459–471. https://doi.org/10.1007/s10584-013-1032-9

Tebaldi, C., Arblaster, J. M., & Knutti, R. (2011). Mapping model agreement on future climate projections. *Geophysical Research Letters*, *38*, L23701. https://doi.org/10.1029/2011GL049863

Vincent, L. A., Wang, X. L., Milewska, E. J., Wan, H., Yang, F., & Swail, V. (2012). A second generation of homogenized Canadian monthly surface air temperature for climate trend analysis. *Journal of Geophysical Research*, *117*, D18110. https://doi.org/10.1029/2012JD017859

Wilcox, E. M., & Donner, L. J. (2007). The frequency of extreme rain events in satellite rain-rate estimates and an atmospheric general circulation model. *Journal of Climate*, *20*(1), 53–69. https://doi.org/10.1175/jcli3987.1

References From the Supporting Information

Wang, X. L., & Feng, Y. (2013). RHtestsV4 User Manual. Climate Research Division, Science and Technology Branch, Environment Canada, Toronto, Ontario, Canada (29 pp.). Retrieved from http://etccdi.pacificclimate.org/software.shtml